2018

Permafrost thaw-induced forest to wetland conversion: potential impacts on snowmelt and basin runoff in northwestern Canada

Emily Haughton
haug6220@mylaurier.ca

Permafrost thaw-induced forest to wetland conversion: potential impacts on snowmelt and basin runoff in northwestern Canada

By

Emily Haughton

(BA. Geography, Wilfrid Laurier University, 2013)

THESIS
Submitted to the Department of Geography and Environmental Studies

In partial fulfillment of the requirements for the
Masters of Science in Geography
Wilfrid Laurier University
Waterloo, Ontario, Canada, 2018

ABSTRACT

In the discontinuous permafrost zone of northwestern Canada, snow covers the ground surface for over half the year, thus snowmelt constitutes a primary source of ecosystem moisture supply and strongly influences stream hydrographs. The peat landscapes along the southern limit of discontinuous permafrost are dominated by forested permafrost plateaus ("forest"), and treeless, permafrost-free wetlands ("wetland"). Permafrost-thaw induced transformation of this landscape has changed water flow and storage processes and therefore introduced new uncertainties on the region's water futures. Here, I a) characterize forest and wetland water storage and flow from snowmelt, and b) evaluate how permafrost thaw-induced wetland expansion at the expense of forest might affect the proportion of snowmelt that can contribute to basin runoff during the spring freshet of a 152-km^2 watershed in the southern Northwest Territories. Analysis of historical imagery suggests that wetland coverage within a 0.14-km^2 area-of-interest increased by approximately 7 % between 1977 and 2010. Over the 34-year period, total areal SWE decreased by 1.5 %, but the amount of SWE made available as runoff increased by 25%. The increased proportion of the snow cover that contributes melt water to streams may be a factor contributing to the rising steam flows observed across the study region in the mid-1990s and early 2000s, given that there has been no concomitant increase in winter-time precipitation.

Contents

Acknowledgements:

I would like to take this opportunity to thank my supervisor, Dr. Bill Quinton for his much needed guidance and support throughout my graduate studies. I am ever grateful for the wealth of knowledge and skills you have bestowed to me through my time working with you.

I would like to thank the many Scotty Creek researchers and members of the Quinton Lab for all of their help in and out of the field. Special thanks to Ryan Connon for assistance in my 2014 and 2015 data collection; I don't know what I would have done in (and out of) the field without your much needed help. I would also like to thank Bhaleka Persaud, Nick Wilson, Clara Greig and Allison McManus for their help and support; my Master's experience would not have been the same without you.

I would now like to thank the many friends and family members who helped me achieve my Master's degree. Specifically, my Mum and Dad, as well as my sister Karli for allowing me to live in her garden gazebo while I was writing a portion of this.

Thank you Kristie Cole for the many hours of discussion, words of wisdom, much-needed pep talks and guidance throughout my Master's degree.

List of Tables

List of Figures

Figure 3. Scatterplots illustrating measured and computed daily total melt rates in mm for WL, SF, and DF sites in **(a)** 2014; R^2 = 0.73, 0.74, 0.51 and **(b)** 2015; R^2 = 0.85, 0.76, 0.68.

Figure 4. (a) Scatterplot illustrating agreement between total daily snowmelt energy and modelled total daily K↓, both in megajoules for the various transect locations (WL>SF> >DF; R^2 = 0.64 to 0.87). Scatter plots illustrating relationship between computed daily snowmelt and total daily measured K↓ for **(b)** 2014 and **(c)** 2015. K↓ was found to be the dominant flux contributing to snowmelt for all land cover types studied.

Figure 5. Line plot illustrating cumulative snowmelt energy in megajoules for the 2014 and 2015 periods of study for wetland, sparse forest, and dense forest land cover types.

Figure 6. (a) Location of trees combined and distribution of incoming solar radiation to the ground for the study periods in megajoules. **(b)** Image presents 0.14 km^2 AOI illustrating routinely surveyed snow transects, location of meteorological stations used in study, as well as the distribution of snowmelt energy in megajoules based on cumulative daily modelled incoming shortwave radiation receipt to the ground.

Figure 7. Composite hydrograph of Jean-Marie River for the time periods 1976-1985 and 2006-2015.

Chapter 1:

General Introduction

1.1 Introduction and background

The southern Northwest Territories (NWT), Canada, is one of the most rapidly warming regions on Earth (Jorgenson *et al*., 2010; Vincent *et al*., 2015), and there is mounting evidence that this warming has affected water resources in this subarctic region. For example, the frequency of mid-winter melt events has increased (Putkonen *et al*., 2009), end-of winter melt occurs earlier (Pachauri and Reisinger, 2007), and key hydrological and climatic variables such as snowpack depth (Hinzman *et al*., 2005), river discharge (St. Jacques and Sauchyn, 2009), and seasonal precipitation patterns (Putkonen *et al*., 2009) have deviated from long-term means. Such changes also have the potential to bring about dramatic changes to subarctic ecosystems with potentially important but poorly characterised feedbacks to hydrological processes. Recent work in the wetland-dominated, southern fringe of discontinuous permafrost or "fringe zone" (Kwong and Gan.,1994), has demonstrated that: 1) the major land cover types have contrasting hydrological functions (Quinton *et al.*, 2003); 2) the relative proportions and spatial arrangement of these cover types is changing due to climate warming (Quinton *et al*., 2009); and 3) this warming-induced land-cover change is affecting the water balance at basin and regional scales (Trochim, 2010).

In the wetland-dominated areas of the fringe zone, permafrost thaw has led to the loss of forest cover and concomitant expansion of treeless wetland terrain (Chasmer *et al*., 2011; Baltzer *et al*., 2014). In these areas, land cover types can be divided into two classes: 1) permafrost-free wetlands; and 2) forested, permafrost cored peat plateaus. Each of these land cover types exhibits contrasting snow accumulation, snowmelt, and runoff regimes (Wright *et al*., 2009). Since the

end-of winter snowmelt event produces the dominant feature of stream hydrographs in subarctic regions, changes to basin snow covers resulting from permafrost thaw-induced land cover change have the potential to disrupt the hydrological cycle of drainage basins occupying this fringe zone. A logical first step toward understanding the long-term implications of land-cover changes occurring throughout this region on late-winter snow distribution, melt and runoff, is to understand how these land cover types differ with respect to their snow covers and their rates and patterns of snowmelt.

1.2 Land cover types

Ice-rich permafrost in the form of tree-covered peat plateaus are common in the peatlands that cover much of the fringe zone. Here, plateaus occur as forested permafrost islands within a wetland complex of flat bogs and channel fens. The contrasting biophysical properties of these three peatland types gives each a specific role in the water balance of drainage basins. The combination of a relatively large snowmelt water supply and a limited capacity to store water enables plateaus to function primarily as generators of runoff which they direct into their adjacent wetlands (Wright *et al*., 2009). Plateau runoff occurs predominately through the thawed, saturated layer that occupies the region between the water table and the underlying, relatively impermeable frost table. Flat bogs are entirely surrounded by the raised permafrost of the plateaus and are therefore unable to exchange surface or near-surface water with the basin drainage network. Subpermafrost groundwater flow is also restricted due to the low hydraulic conductivity of the underlying clay-rich glacial till. However, recent field studies at Scotty Creek, NWT (Connon *et al*., 2015) found that certain bogs can form lateral surface connections with the channel fen. These bogs can are either connected with the fen network through ephemeral drainage channels that cut through a plateau (*i.e.* cascade bogs) and bogs that have a

direct, open connection with the fen (*i.e.* open bogs). These connected bogs can produce runoff under conditions of high moisture supply and/or minimal ground thaw.

Cascade bogs route water through a series of connected bogs and eventually drain into a fen, and open bogs occur where the permafrost that once separated a flat bog from an adjacent fen has thawed entirely or sufficiently so that the flat bog is now 'open' (*i.e.* hydrologically connected) to the fen. This process referred to as 'bog capture' (Connon *et al*., 2014) enables surface and near-surface flow between fens and open bogs during periods of high moisture supply. Finally, the channel fens collect water from their surrounding peatlands and convey it along their broad (~50-100 m), hydraulically rough channels, toward the basin outlet (Quinton *et al.*, 2003).

1.3 Land cover change

Climate warming disrupts the balance between permafrost aggradation and degradation described by Zoltai (1993) such that permafrost degradation is favoured. For example, 30-65% of permafrost in the fringe zone of the southern NWT has degraded over the last 100-150 years (Beilman and Robinson, 2003), with degradation rates increasing in recent decades (e.g. Lantz *et al*., 2008). The aforementioned loss of forest and expansion of wetlands is driven by permafrost-thaw induced subsidence of plateau ground surfaces which are then flooded by the adjacent bogs or fens (Jorgensen *et al*., 2005). There are strong indications that permafrost thaw and the resulting land-cover changes have affected basin water balances, as suggested by rising river flows throughout the fringe zone (St. Jacques and Sauchyn, 2009). For example, the total annual runoff from all gauged rivers in the lower Liard River valley of the NWT has steadily risen since the mid-1990s (Connon *et al*., 2014), with the exception of very dry years of 2013 and 2014 (MSC, 2016). The current understanding of water flow and storage processes in wetland-

dominated, discontinuous permafrost terrains, and how climate warming and the resulting land cover changes affect these processes, cannot adequately explain this rise in river flows, nor is it sufficient to predict future river flows. Rising flows from subarctic rivers are often attributed to 'reactivation' of groundwater systems (*e.g.* St.Jacques and Sauchyn, 2009), but the very low hydraulic conductivity of the glacial sediments throughout much of the lower Liard River valley precludes appreciable groundwater input. Permafrost thaw-induced changes to basin flow, and storage processes including expansion of runoff contributing areas, offers a more plausible explanation for rising river flows in this region (Connon *et al*., 2014). This increase in lateral surface and subsurface connectivity is especially pronounced during the spring freshet, when infiltration is reduced due to the presence of frozen ground beneath the snowpack. As hydrological connectivity increases it is expected that a greater proportion of snowmelt water will be available to the basin drainage network.

1.4 Snowcover

Snow on the ground plays an important role in the formation and preservation of the permafrost below the plateaus (CWWG, 1988). The depth of the snow cover is strongly influenced by the tree canopy, which intercepts and stores snowfall, which proportionately reduces the snow accumulation on the ground below (Pomeroy and Gray, 1995). Tree canopies also reduce wind speeds over the sub-canopy snowpack (Pomeroy and Harding, 1996), and influence wind speeds and turbulence over adjacent treeless terrains. The erosion, transport, and deposition of snow by wind is highly variable over the mosaic of peat plateaus, fens, and flat bogs. Snow accumulation below tree canopies can be 20 to 45% less than in adjacent open terrains (Golding and Swanson, 1986), with the difference in snow depths between the forested and treeless terrains increasing with the size of the latter due to increased wind erosion in larger

open areas. For example, open areas with a fetch of five times the height of the tree canopy (5H) at the up-wind forest edge, accumulate the maximum amount of snow (Troendle and Leaf, 1980). When the size of the clearing is greater than 12H, the clearing retains less snow compared with the upwind forest floor. The reduction of snow retention with increasing fetch results from the greater likelihood for wind gusts (Pomeroy and Gray, 1995).

Spatial variations in the distribution of snow on the ground and of its melt rate not only have implications for the volume and timing of runoff, but also have the potential to influence the rate and spatial pattern of permafrost thaw, and therefore the spatial pattern of permafrost thaw-induced land cover change, which ultimately feeds back to affect flow and storage processes (Connon *et al*., 2014).

1.5 Snowmelt

The energy balance of the snow surface controls the production of melt water, and is therefore critically important that it be represented accurately in any numerical simulation of snowmelt and runoff. Snowmelt energy balances have been well documented in a variety of cold environments, including prairie (Male and Granger, 1981), alpine (Cline, 1997) and peatland (Knox *et al*. 2012). There has been little study of snowmelt energy balances in the peat plateau-fen-bog dominated landscape of the fringe zone; however, much information can be transferred from studies in other, similar land cover types. For example, treeless surfaces such as wetlands, typically experience greater contributions from turbulent fluxes as a result of higher windspeeds (Male and Granger, 1981). Depending on the size and orientation of the wetland, turbulent fluxes can drastically alter the snowmelt energy balance and snow characteristics of a land cover with increased losses due to wind-driven sublimation as a result of increased contributions from turbulent fluxes (Male and Granger, 1981). Radiative fluxes somewhat contrast those of forested

terrain such that greater maximum incoming radiation occurs, as well as greater losses to longwave in the absence of a moderating medium such as a tree canopy.

The surface energy balance below tree canopies is more complicated, since such canopies are known to provide a larger reflecting, absorbing and radiating structure above the snowcover surface that it interacts with both mass (snowfall) and energy flows. Therefore, the surface energy balance of the snowpack on the plateaus is expected to be strongly influenced by the large spatial variability of radiative and turbulent transfers (Pomeroy *et al*., 2008), and by variations in the structure and density of the forest canopy (Hardy *et al*., 2004; Davis *et al*., 1997; Pomeroy, 2006), which attenuates incoming solar radiation, alters the surface albedo by way of leaf litter deposition, and shelters the snow surface from wind. The latter reduces the amount of energy available for melt by dampening turbulent fluxes, making snowmelt dependent mainly on radiative fluxes (Boon *et al*., 2009; Davis *et al*., 1997; Sicart *et al*., 2003).

Conifer tree canopies also introduce irregularities in the spatial distribution of energy applied to the snow surface which, during the annual snowmelt event, can influence the rate of snow cover depletion and the areal mean snowmelt rate at small, sub-stand scales (Faria *et al*., 2000). For example, absorption of shortwave radiation by trunks and branches, and its redistribution as longwave energy, affects the spatial and temporal distributions of melt energy (Golding and Swanson, 1986; Verry *et al*., 1983; Woo and Geisbrecht, 2000). Longwave radiation creates 'hot spots' around trees that produce patches of bare ground extending outward from the trunk in the direction of melt (Davis *et al*., 1999; Hardy *et al*., 2004). The spatial distribution of these hot spots is determined by that of the tree trunks (Rowlands et al., 2002). This process is especially pronounced in stands containing a significant number of dead or dying trees (Pomeroy *et al*., 2009), as observed on the subsiding edges of thawing peat plateaus, since

such trees warm more readily than healthy trees owing to their relatively low moisture content and lower volumetric heat capacity (Vines, 1968).The spatial distribution of incoming shortwave energy arriving at the sub-canopy snow surface is large and varies continually throughout the day due to changing sun angles through a heterogeneous canopy (Sicart *et al*., 2003). Spatial patterns of snowmelt are often controlled by the spatial variation of shortwave radiation arriving at the sub-canopy snowpack surface (Pomeroy *et al*., 2008). Since snowmelt is the primary source of runoff to streams in the subarctic, canopy characteristics such as stand density and spatial extent must have an indirect effect on landscape runoff and streamflow. For example, changes to canopy structure and density or aerial extent of the stand can change the amount of snow intercepted by the canopy and therefore the amount that would subsequently sublimate back to the atmosphere (Burles and Boon, 2011; Pomeroy *et al*., 2012), thereby changing the water equivalent of the sub-canopy snowpack, and the amount of moisture available for runoff (Pomeroy *et al*., 1993). The permafrost thaw induced changes to tree canopies reported for the southern margin of discontinuous permafrost including canopy thinning (Baltzer *et al*., 2014), and the conversion of forests to wetlands (e.g. Robinson and Moore, 2002), have potentially important but poorly understood implications to basin runoff.

1.6 Thesis Overview

The thesis consists of one manuscript which examines the effects of permafrost thaw - induced land cover changes on basin snowmelt runoff production. This goal is met by a) characterising the snow water equivalent (SWE) storage and melt of forested and treeless land cover types for the 2014 and 2015 hydrological years and b) evaluating how the permafrost thaw-induced wetland expansion and resulting forest loss might affect the aerially weighted

SWE storage, and the proportion of snowmelt that can contribute to basin runoff during the spring freshet over the time period 1977-2010.

A brief summary of the main research findings and an explanation of the implications of permafrost thaw-induced land cover changes on SWE storage and melt concludes the thesis. Furthermore, the final chapter identifies gaps in the existing body of scientific knowledge on the subject of permafrost degradation and presents recommendations on potential areas for future research.

Chapter 2: Permafrost thaw-induced forest to wetland conversion: potential impacts on snowmelt and basin runoff in northwestern Canada

E.R. Haughton[1], L. Chasmer[2], R. Connon[1], O. Sonnentag[3], W.L. Quinton[1]

[1]Cold Regions Research Centre, Wilfrid Laurier University, Waterloo, ON, Canada,
[2]Department of Geography, University of Lethbridge, Lethbridge, AB, Canada.
[3]Departément de géographie & Centre d'études nordiques, Université de Montréal, Montréal, QC, Canada,

2.1 Introduction:

Northwestern Canada is one of the most rapidly warming regions on Earth (IPCC AR5, 2014). It is expected that continued warming will have a substantial influence on snow accumulation, (re-) distribution and melt patterns in this region, resulting in greater frequency of mid-winter snow melt events (Putkonen *et al*., 2009), a shorter snow-covered season (Semmens *et al*., 2013; Pachauri and Reisinger, 2007), and greater variability in snow depth (Hinzman *et al*., 2005). Such changes throughout northwestern Canada co-occur with warming-induced permafrost thaw (Connon *et al.,* 2014; Goodrich, 1982), resulting in changes to active (i.e. seasonally frozen and thawed) layer properties (Sturm *et al*., 2005) and ecosystem composition, structure and functioning (Jorgensen *et al*., 2001). The combined effects of such snow cover, permafrost and ecosystem changes on water storage and flow is poorly understood, and as a result, there is considerable uncertainty on the future availability of water resources in the region (NWT Water Stewardship Strategy, 2009).

The highest rates of aerial permafrost thaw in northwestern Canada are found in the region near the southern limit of discontinuous permafrost, since the permafrost in this low-

lying, peat-dominated 'fringe region' (Kwong and Gan, 1994) is relatively thin (< 15 m), and is at or near the freezing point depression temperature (-0.3°C). Moreover, its spatially discontinuous nature allows thaw to be driven by both vertical heat flows from the ground surface and horizontal heat conduction and advection from the permafrost edges. Much of the fringe region occurs below forested plateaus ("forest") which are surrounded by and often contain permafrost-free, treeless wetlands ("wetland"). Specifically, such forests may occur as a relatively small "islands" (<400 m^2) within a larger wetland, but more often forests are sufficiently large that they contain numerous treeless wetlands 'collapse-scar bogs'. Because of their higher (1-2 m) topographic position, sloping surfaces, and the presence of permafrost near the ground surface, water drains from the forests to the wetlands (Quinton and Baltzer, 2013). Since the wetlands are impounded by the raised permafrost of the surrounding forest (Quinton *et al*., 2003), water loss from these features and the overall landscape is typically controlled by evaporation (Helbig *et al*., 2016a) and groundwater recharge (Gordon *et al*., 2016). Forests containing wetlands (*i.e.* forest-wetland complexes) are typically bordered by open channels, riverine wetlands or channel fens, which collectively comprise the basin drainage network. Water received by this network from the forest-wetland complex is conveyed slowly toward the basin outlet (Quinton et al., 2009).

Permafrost-thaw induced land cover change is well documented in the zone of discontinuous permafrost in northwestern Canada (*e.g.* Helbig *et al*., 2016b; Quinton *et al*., 2011; Robinson and Moore, 2002). Permafrost thaw and associated melting of ground ice causes subsidence of the overlying ground surfaces which are then engulfed by the surrounding wetlands (McClymont *et al*., 2013). Through this permafrost thaw-subsidence-flooding sequence, forests are transformed into permafrost-free wetlands. Between 30 and 65 % of the

permafrost-supported forest has disappeared from this region over the last 100 to 150 years (Jorgensen *et al*., 2001), with concomitant increases in wetland coverage (Chasmer *et al*., 2010). Annual forest-to-wetland conversion rates have increased in recent decades (Chasmer and Hopkinson, 2016) as the forests have become more fragmented, resulting in increased edge-to-area ratios (Baltzer *et al*., 2014).

It is reasonable to expect that the conversion of forest to wetland will itself transform the end-of-season snow cover distribution, since the areal average snow cover is known to decrease as the proportion of open land cover increases (*e.g.* Pomeroy and Gray, 1995), owing to the differences between forested and treeless land cover types in terms of snow interception (Faria and Pomeroy, 2000), sublimation (Storck *et al.,* 1999), and surface energy balance (Helbig et al., 2016b). Such a forest-to-wetland conversion is potentially of great importance hydrologically for the fringe region, where the end-of-winter snowmelt event releases roughly half of the total annual precipitation within a two to three-week period at a time when infiltration and storage are limited by frozen ground (Woo, 1986).

Aside from inducing a forest-to-wetland conversion, permafrost thaw also alters the hydrological connectivity of the landscape. For example, the thaw of permafrost separating a wetland from the basin drainage network transforms the wetland from being internally drained to one hydrologically connected to the basin outlet. As such wetlands expand due to permafrost thaw around their margins, they merge into other wetlands, a process that further expands the basin runoff contributing area, and therefore basin runoff as well. Thawing permafrost has also led to the formation of drainage channels between wetlands, allowing them to transmit overland and shallow subsurface runoff along a wetland cascade toward the basin drainage network and onward to the basin outlet (Connon *et al*., 2015).

By converting forests to wetlands and by increasing the hydrological connectivity of the landscape, permafrost thaw has the potential to affect snow accumulation, melt, and snowmelt runoff processes, with implications to the volume and timing of the hydrograph response of basins during the spring freshet. St. Jacques and Sauchyn (2009) demonstrated significant increases in mean annual stream flow in the sporadic and discontinuous permafrost zones of the Northwest Territories (NWT), Canada. These authors suggest that groundwater reactivation as a result of permafrost thaw may cause these increases. However, a widespread, clay-rich glacial till deposit with very low hydraulic conductivity exists beneath the peatland complexes in the southwestern NWT (Hayashi *et al.,* 1998), suggesting that groundwater reactivation may not be the primary driver of rising stream flows in this region. Connon *et al*. (2014) suggested that permafrost thaw is increasing stream flows through increased surface and near-surface hydrological connectivity.

Using continuous, year-round micrometeorological measurements, snow surveys, and simple snow surface energy balance calculations, the goal of this study is to evaluate the impact of permafrost thaw-induced land cover changes on basin snowmelt runoff production. This goal is met by a) characterising the snow water equivalent (SWE) storage and melt of forested and treeless land cover types for the 2014 and 2015 hydrological years and b) evaluating how the permafrost thaw-induced wetland expansion and resulting forest loss might affect the aerially weighted SWE storage, and the proportion of snowmelt that can contribute to basin runoff during the spring freshet.

2.2 Study Site:

Scotty Creek (61°18' N, 121°18' W) is a 152 km^2 drainage basin that lies 50 km south of Fort Simpson in the lower Liard River valley of the NWT, Canada (Figure 1a). Hydrometric data

at Scotty Creek has been collected by the Water Survey of Canada (WSC) since 1995. Longer term hydrometric records (1972 to present) are available for the adjacent 1 310 km^2 Jean-Marie River basin, an area that exhibits similar land cover characteristics and hydrologic response to the Scotty Creek basin (Quinton *et al*., 2003; Connon *et al*., 2014). The longer term hydrometric data allows for the analysis of changing runoff patterns as a response to permafrost thaw. Annual runoff at Jean-Marie river over the past 30 years (1986 – 2015) is 143 mm yr^{-1} (WSC, 2017), while a significant increase in runoff has been observed since 1996 (Connon *et al*., 2014).

The landscape of the southern portion of the Scotty Creek basin is underlain by discontinuous permafrost (Hegginbottom and Radburn, 1992) and is comprised of peatland complexes typical of the 'continental high boreal' wetland region (NWWG, 1988). The Scotty Creek drainage basin has a thick peat cover (2-8 m, McClymont *et al*., 2013) overlying a thick clay/silt-clay glacial till deposit of low permeability (Aylesworth and Kettles, 2000; Hayashi *et al*., 1998). Most of the Scotty Creek basin is a heterogeneous mosaic of forested peat plateaus underlain by permafrost ('forest'), and treeless, permafrost-free wetlands ('wetland') (Figure 1b), typical of the southern fringe of discontinuous permafrost (Helbig *et al*., 2016a). This study focuses on a 0.14 km^2 area-of-interest (AOI) with 40% forest and 60% wetland coverage (Figure 1c). Measurements were made at fixed, individual points and along measurement transects within the forest and wetland portions of the AOI (Figure 1b). The AOI included 40 wetlands ranging in size between 1,000 m^2 and 20,000 m^2. The plateaus support a black spruce (*Picea mariana*)-dominated canopy with an average tree height of 3.1 m (Chasmer *et al*., 2010), as well as multiple shrub species including Labrador tea *(Ledum groenlandicum*), small bog cranberry (*Vaccinium oxycoccos*), Leatherleaf (*Chamaedaphne calyculata*), bog birch (*Betula glandulosa*), and a variety of lichen and moss species on the ground surface (Gabron-Labreque *et al*., 2015).

In the wetlands, the vegetation consists of mosses (*Sphagnum fuscum*, *Dicranum elongatum*) and non-tussock forming stands of sedges (*Eriophorum vaginatum*). The Fort Simpson region has a dry continental climate with short, dry summers and long, cold winters. Based on climate normals (1971-2000), mean annual air temperature is -3.2^{o} C, with 369 mm of annual precipitation, of which 46% falls as snow (MSC, 2016). Snowmelt usually commences in the early to mid-April and continues throughout most of the month, so that by May, only small amounts of snow remain (Hamlin *et al*., 1998).

2.3 Methods:

The AOI was separated into large wetland (LW), small wetland (SW), sparse forest (SF) and dense forest (DF) classes. The distinction between small and large wetlands was based on a non-parametric Kruskal-Wallis H-test (Kruskal and Wallis, 1952) of the end-of-winter snow water equivalent of 40 wetlands within the AOI in addition to a histogram analysis, in which the median wetland area (10, 000 m^2) was selected as a threshold for separation. Using nine years of data between 2006 and 2015, this test indicated that the SWE of wetlands larger than approximately 10,000 m^2 (WL) have significantly lower SWE values than forests ($H = 10.31, df = 3, \alpha = 0.05$), while wetlands smaller than 10,000 m^2 (SW) have SWE values not significantly different than those of the forest cover Using these results, the 40 wetlands of the AOI were separated into 14 of the LW class and 26 of the SW class. The Kruskal-Wallis H-test indicated no significant difference between SF and DF in terms of SWE, however the distinction was made because stand density is known to affect the amount of radiation reaching the snow and ground surface below the canopy. In this study, we defined SF as having a stem density of 1 - 2 stems m^{-2}, and DF as having stem densities greater than 2 stems m^{-2} based on stem counts

done along each snow survey transect. Using these values, the forested portion of the AOI was separated into SF and DF classes through stem counts along the routinely surveyed transects.

Meteorological stations were located in SF, DF and LW areas of the AOI. The LW station was assumed to represent the meteorological conditions of both the LW and SW classes. At each station, air temperature (T_a; °C) and relative humidity (RH; %) were measured with a temperature-relative humidity sensor enclosed in a radiation shield (HMP4C5; Vaisala, Helsinki, Finland). Wind speed (U_z; m s^{-1}) was measured using standard cup anemometers (O14A; Met One Instruments INC, Grants Pass, Oregon, USA) at 1.5 m above the mean ground surface. Snow depth (d_s; m) was measured using a snow depth sensor (SR50A; Campbell Scientific, Logan, Utah, USA). Net radiation (Q_{net}; W m^{-2}) and incoming and outgoing short and longwave radiation were measured with a four-component net radiometer (CNR1; Kipp & Zonen, Delft, the Netherlands) at 1.5 m above the ground surface. Snowpack temperature was measured using four thermistors (109; Campbell Scientific, Edmonton, Alberta, Canada) vertically spaced at 10 cm intervals, with the deepest sensor located at 10 cm above the ground surface. All other station measurements were taken every minute and averaged and recorded every half hour. All station measurements were recorder using a CR1000 data logger (Campbell Scientific).

To characterize melt, snow surveys were conducted along seven 100-m transects representing the SF, DF and LW classes every other day throughout the snowmelt period in 2014 (10 measurement days) and 2015 (14 measurement days) (Figure 1b). Along each transect, snow depth was measured every metre using a ruler following the standard method described by Pomeroy and Gray (1995). Snow samples of known volume were taken every 5th depth measurement using the standard federal snow tube (Geo Scientific; Vancouver, BC, Canada) and weighed with an electronic scale (Light Duty Crane Scale; BC Scale, Langley, BC, Canada) to

determine snow density. Average depth and density measurements were used to compute average SWE for each transect. Each transect was equipped with three ablation stakes, located next to the first, middle, and last transect point (Wright et al., 2008). Daily ablation was derived from the change in the elevation of the snow surface, relative to the fixed datum of the ablation stake over a 24-hour period. Snow density was also measured in the vicinity of the ablation stake, but far enough away (5 to 10 m) to not impact the ablation measurements. The ablation stakes were used to compute the depth of daily melt, as well as provide a spatially distributed set of data independent of the transect.

2.3.1 Snowmelt Energy Balance:

The snow surface energy balance was computed with data supplied by the LW, SF and DF stations using the one-dimensional energy balance equation:

$$Q_m = Q* + Q_h + Q_e + Q_g - Q_{cc} \qquad (1)$$

where Q_m is the energy available for snowmelt, Q_h and Q_e are the turbulent fluxes of sensible and latent heat, Q_g and Q* is the net all-wave radiation. All units are MJ m^{-2}. When the snow surface is melting, the air directly above is assumed to have a temperature of 0°C and a vapour pressure at the saturation value of 6.11mb (Heron and Woo, 1978). The horizontal wind speed is assumed to be zero at the snow surface, and increase logarithmically to the measurement height above the snow.

Q_h was calculated as a function of the difference between the temperature at the snow surface and overlying air as:

$$Q_h = p_a C_{pa} D_h (T_a - T_{ss}) \qquad (2)$$

where p_a is the density of air (kg m^{-3}), Cp_a is the heat capacity of air at a constant pressure (J $kg^{-1}K^{-1}$), D_h is the bulk sensible heat transfer coefficient (m s^{-1}), and T_a and T_{ss} are the temperatures of the air and snow surface (K).

Q_e was calculated as a function of the difference in vapour pressure in the overlying air as:

$$Q_e = p_a \lambda_v D_e \frac{0.622}{P}(e_a - e_{ss}) \quad (3)$$

where λ_v is the latent heat of vapourization (2.48x10^6 J kg^{-1}), D_e is the bulk latent-heat transfer coefficient (m s^{-1}), P is the atmospheric pressure (kPa) and e_a and e_{ss} are atmospheric and snow surface vapour pressures (kPa). Positive Q_e values indicate energy directed into the snowpack as condensation, while negative Q_e values indicate energy release from the snow surface through either evaporation or sublimation.

Q_g can be estimated using soil temperature and moisture data (Gray and Prowse, 1993):

$$Q_g = k_g\left(\frac{\Delta T_s}{d_s}\right) \quad (4)$$

where k_G is the thermal conductivity of the soil (W m^{-1} K^{-1}), ΔT_s is the change in temperature of the soil (K), and d_s is depth of measurement below the ground (m). The ground heat flux at this site was deemed negligible.

Q_{cc} is the change of internal energy in the snowpack (Gray and Prowse, 1993). Within deep snowpacks internal energy changes can be relatively small in comparison to other energy fluxes and in most studies are considered negligible because the snowpack temperature during ablation is close to 0ºC. However, if snow melts during the day and freezes overnight, large changes in internal energy can occur within shallow snowpacks and the upper layers of deep snow. Q_{cc} is calculated using:

$$Q_{cc} = -c_i p_w h_m (T_s - T_m) \quad (5)$$

where c_i is the heat capacity of ice (2102 J kg^{-1} K^{-1}), T_s is the average temperature of the snowpack, T_m is the melting point of ice (0^oC), ρ_w is the density of water (approximately 1000 kg m^{-3}), and h_m is the snowpack water equivalent in meters.

In a constant flux layer, under the assumption of neutral atmospheric conditions, the diffusivities of water vapour and heat can be seen as equal (Dingman, 2002) such that $D_h=D_e=D$ and:

$$D = \frac{k^2 u_a}{\left[\left[ln\frac{z_a}{z_o}\right]\right]} \quad (6)$$

where k is von Karman's constant (0.4), u_a is the windspeed (m s^{-1}), z_a is the height of the wind measurement (m) and z_o is the surface roughness (m) of the snowpack. Surface roughness refers to an estimation of the mean height of the roughness elements of the snow surface. The values of z_o should theoretically incorporate the increasing roughness of the snow surface as the ablation season progresses, and as snow cover becomes patchy and vegetation appears (Metcalfe and Buttle, 1998) however following the results of a sensitivity analysis conducted by Boon (2009), it was found that z_o was relatively insensitive within an order of magnitude in healthy forest stands.The surface roughness coefficient of 0.006 m was used as it represents a midway value between seasonal (0.005m) and wet (0.006m) snow covers, and was deemed representative of the snow characteristics at the study site (see Moore, 1983; Oke, p.57, 1988).

The Richardson number (Ri) was used to characterize the stability of the atmospheric boundary layer (Dingman, 2002):

$$Ri = \frac{g[T_a - T_{SS}]}{u_a^2 \ T_k} \quad (7)$$

where g is acceleration due to gravity (ms^{-1}) and T_k is the mean temperature of the air (K). Temperature inversions often occur over snow cover and create stable conditions as temperature increases with increasing altitude suppressing turbulence. As the temperature of the snow surface

has been fixed to 0°C, T_a-T_{ss} is usually positive, indicating stable atmospheric conditions over the snowpack. To correct for the occurrence for stable conditions (*i.e* Ri>0.3), D_h and D_e were modified following the method of Price and Dunne (1976):

$$D_{MS} = \frac{D_M}{1+10Ri} \quad (8)$$

When the atmosphere was unstable (*i.e.* Ri<0.3), the bulk transfer coefficient was modified following the method of Price and Dunne (1976):

$$D_{MU} = D_M(1 - 10Ri) \quad (9)$$

Daily total snowmelt was computed using the following equation:

$$M = \frac{Q_m}{l_v} \quad (10)$$

where M is the amount of snowmelt over a 24 hour period in mm and l_v is the latent heat of fusion in MJ m^{-2}.

For each meteorological station, the cumulative measured value of incoming shortwave radiation (K↓) was regressed with the total daily Q_m computed value over the same 24-hour period. The relationship derived for the LW station was assumed to represent both LW and SW classes. Each relationship was then used to estimate the total daily Q_m within each land cover class from the distributed values of direct K↓ provided by Solar Analyst (ArcGIS 10.1; ESRI, Redlands, CA, USA). This procedure was conducted using a pixel resolution of 1 m for the period 1 April to 10 June in both 2014 and 2015, and verified from digital aerial photography following Chasmer *et al*. (2011). The values of direct K↓ provided by Solar Analyst were added to diffuse K↓ estimated using an atmospheric transmissivity multiplier of 0.5. In order to verify the accuracy of the distributed Q_m estimates, the total *(i.e.* direct + diffuse) K↓ values were extracted for each pixel along the snow survey transect (T) representing the SF (T1), DF (T2) and LW (T3) land cover components. These extracted values were then summed for each pixel

along each transect for each day of the 2014 and 2015 snowmelt periods and converted to total daily Q_m values based on the regressions developed by the procedure described above. The resulting estimates of total daily melt for each transect were then compared with the day to day measured change in SWE for the same transects.

The permafrost thaw induced change in forest and wetland cover between 1977 and 2010 reported by Connon *et al*. (2014) for the same AOI as used in this study, was used to evaluate how permafrost thaw affects the aerially weighted SWE, and the proportion of the SWE that can contribute to basin runoff during the spring freshet. In the present study, "Connected SWE" refers to the snow cover of an area that is hydrologically connected to the basin drainage network and "isolated SWE" refers to snow cover of an area that is hydrologically isolated from the drainage network. To evaluate the impact of the permafrost-thaw induced increased connectivity of the landscape on streamflow, the ratio between total precipitation input and total runoff (*i.e.* the runoff ratio) was computed for Scotty Creek and the adjacent Jean-Marie River basin for the snowmelt runoff period (1 April to 30 May) and for the summer period (1 June to 31 September). Runoff from both watersheds was measured by the Water Survey of Canada and precipitation was measured at the Fort Simpson A climate station. Total annual snowfall was also computed to evaluate whether changes in winter precipitation have occurred over the same period (1977-2010).

2.4 Results:

2.4.1 Snow accumulation:

The two years in this study received a stark difference in snowfall amount, allowing for comparison between years with high and low end-of-season SWE. There was 95.6 mm of SWE in 2014, the second-lowest amount over the past 30 years, as recorded by Environment Canada

at the Fort Simpson A station. In contrast, the 2015 winter received 167.0 mm, well above the 30-year average of 138.6 mm in Fort Simpson (Table 1). These values recorded in Fort Simpson have not been corrected for gauge undercatch, but allow for comparison to the 30-year climate normal. Snowfall was also measured at the study site using a Geonor weighing gauge and undercatch was accounted for by the method of Smith (2008). At the study site, total adjusted snowfall was 143.7 mm in 2014 and 216.6 mm in 2015.

Snow surveys conducted near the end of the snowfall season (late March) displayed similar results. In 2014, the average end of season snowpack in WL areas was 95.8 mm, while forested areas (SF and DF combined) retained 99.1 mm of SWE. In 2015, WL sites had 170.8 mm of SWE and forests had 179.9 mm of SWE. The trend observed here of forested sites retaining marginally more end-of-season SWE than WL sites is consistent with the previous 15 years of snow survey data from the study site.

Given the large differences in end of season SWE, snow depth at the WL sites was surprisingly similar between years, with average depths of 60.1 cm in 2014 and 69.5 cm in 2015 (Figure 2). The similarities in snow depth were offset by large differences in snow density. Average density in 2014 was 0.159 g cm^{-3}, whereas the average density in 2015 was 0.246 g cm^{-3}. The similarity in depth and disparity in density in the WL sites is likely a result of a string of warm temperatures at the end of March, 2015. It appears that the warm temperatures caused an internal collapse in the snowpack, as is shown in Fig 2b. Meltwater likely infiltrated into and percolated through the snowpack, eventually consuming large amounts of latent heat upon re-freezing. This energy consumption within the snowpack likely led to structural instability in the depth hoar-base and caused the collapse.

A more noticeable difference was observed in average snow depth at forested sites, with 2014 having an average of 58.4 cm and 2015 receiving 77.7 cm. The average density at forested sites was 0.170 g cm^{-3} in 2014 and 0.232 g cm^{-3} in 2015. Of the 143.7 mm of SWE that fell in 2014, 10.5 mm of SWE fell after snow surveys were conducted. In 2015, 28.0 mm of the 216.6 mm of SWE fell after the completion of snow surveys. As expected, end of season SWE on the ground is less than the total recorded snowfall, largely due to wind-blown sublimation loss in open wetland areas, and canopy interception and subsequent sublimation in forests.

In addition to the drastic differences in total snowfall amount, there was also a noticeable difference in the amount of snow retained on the ground. In 2014, at the time of snow surveys, WL sites had retained 72% of total snowfall, while forested sites retained 74%. Conversely, in 2015, WL sites had 91% of total snowfall, and forest sites had 95%. This is likely explained by differences in canopy sublimation rates. The unloading of intercepted snow from tree canopies increases with time and with the load stored (Hedstrom and Pomeroy, 1998). This suggests that in years with low snowfall amounts, there is a decreased probability of canopy unloading. Sublimation rates within a canopy can be very high (Schmidt 1991, Pomeroy *et al*., 1998), which decreases the amount of snow that is retained in the end of season snow cover, and ultimately the amount of moisture available for the spring freshet. Timing for snow accumulation was also very different between the two years (Table 2). In 2014, the most of the snowfall (74%) occurred in the middle of the winter (November, December, and January). In 2015, only 34% of total snowfall occurred during these months. Large snowfall events occurred near the start and end of winter, where warmer temperatures allow for increased amounts of atmospheric moisture.

2.4.2 Snowmelt:

The duration of snowmelt was much higher in 2015 than 2014, due primarily to the difference in snowpack size and the amount of extra energy required for melt. The onset of snowmelt (defined as the day when the snowpack became homogenous and isothermal determined from snow pit analysis) in 2014 occurred approximately 10 days later than in 2015, due to relatively cool April air temperatures. Average April temperatures in 2014 were -2.3°C in 2014, compared to 1.4°C in 2015. In both years, snowmelt was most rapid in WL sites and was prolonged in the SF and DF sites (Table 2). The difference in snowmelt onset and duration between land cover types exerts a key control on the quantity and timing of snowmelt water during the freshet.

Snowmelt values calculated using the snow surface energy balance matched closely with measured values for each land cover type during both years of study (Figure 3). The validation of the snow surface energy balance calculations allows for a comparison of the contributing fluxes to Q_m. While computed and measured values are in relatively close agreement ($p < 0.05$) in both years of this study, computed melt was less accurate in 2014. The relatively shallow snowpack in 2014 became discontinuous early in the melt period, enabling advective energy contributions from snow-free patches. This was caused by a reduction in surface albedo and subsequent increased absorption of solar radiation by the ground and ground heat flux early in the year (Granger *et al*., 2006). Moreover, a patchy snow cover increases the surface roughness as vegetation protrudes through the snow cover, a phenomenon not accounted for in the snow melt computations. In addition, the Richardson stability correction introduces error in the underestimation of the turbulent fluxes that could be greater when compared to the wetlands due to the frequency of extremely stable atmospheric conditions experienced throughout both 2014 and 2015 melt periods (Andreas et al., 2002).

In both years and at all land cover types, Q^* was the dominant flux contributing to Q_m (Table 4). Combined, the two turbulent fluxes (Q_h and Q_e) account for between 12 and 32% of Q_m. Of the four components contributing to Q^*, $K\downarrow$ contributed the largest amount of energy to Q_m, indicating that melt in the region is driven primarily by $K\downarrow$ (Table 4). The average cumulative $K\downarrow$ for the melt season expressed as a fraction of the total cumulative Q_m over the same period (*i.e.* $\Sigma K\downarrow/\Sigma Q_m$) for the three sites was 0.70 in 2014 and 0.78 in 2015.

Typically, the upward longwave flux ($L\uparrow$) is greater than the downward flux ($L\downarrow$) such that L^* represents a loss from the snowpack. Of the three land cover types, the DF site received the highest contribution from L^*, which was likely due to the emission of longwave radiation from the relatively warm trees. At these locations, L^* contributions were slightly less than the WL sites, however this increase in longwave energy was not substantial enough to counter-act the decrease of shortwave radiation imposed by the tree canopy.

Because of the strong control that $K\downarrow$ exerts on snowmelt, an incoming radiation model was used to simulate snowmelt across the AOI. The $K\downarrow$ values produced by the model produced values that matched closely with values measured at the meteorological stations at the three site types, with the strongest association at WL sit (R^2 : 0.98), owing to the absence of a tree canopy. The root mean square error (RMSE) was lowest at the WL site (0.34 and 0.14 MJ for 2014 and 2015, respectively), highest for the DF site (2.12 and 2.65 MJ) and moderate for the SF site (1.77 and 1.80 MJ). Total daily modelled K↓ was closely correlated to total daily snowmelt measured along each snow survey transect (Figure 4). The cumulative modelled Q_m for the snowmelt period ranged between 72 and 106 MJ for the WL areas of the AOI, 106 and 140 MJ in SF areas, and between 140 and 174 MJ in DF areas (Figure 5).

2.5 Discussion:

2.5.1 Comparison of energy dynamics between forest and wetlands:

Turbulent fluxes of sensible and latent heat play an important role in snow surface energy and mass balances which change with differing land cover characteristics (Marsh and Pomeroy, 1996; Link and Marks, 1997; Koivusalo and Kokkonen, 2006). Trees reduce wind speed and subsequently reduce the exchanges of latent and sensible heat between the snow pack and the overlaying atmosphere, making the forest canopy an important factor influencing the snow surface energy balance (Pohl et al., 2006; Knox et al., 2012). Conversely, open areas, such as wetlands, typically receive greater solar radiation, and experience greater loss of longwave radiation (Marks *et al*., 1998). These patterns were observed in this study, which showed that ~70 to 80% of net radiation was available as melt energy. The analysis of modelled K↓ illustrates that the range of K↓ captured by the model is more variable in the SF and DF sites than WL sites due to the forest canopy (Figure 6.) Subsequent irregularities in K↓ are introduced as a result of variable canopy gaps and canopy scattering elements (Faria et al., 2000) with SF sites consistently receiving higher inputs of K↓ compared to the DF sites (Figure 6). These patterns become very pronounced in more southern regions where closed canopies reduce K↓ at the ground surface relative to open sites (Hardy *et al*., 2004; Ellis and Pomeroy, 2007; Pomeroy *et al*., 2007; Lawler and Link, 2011). The irregularities in canopy gaps studied here result in uneven snowmelt patterns within forest patches.

Differing snowmelt patterns between land cover types allowed WL sites to be the first to experience snow-free conditions while less snow accumulation in WL sites meant that energy requirements to melt the snowpack were lower than in SF and DF sites (Figure 5). These findings are consistent with other studies conducted in similar environments (Koivusalo and

Kokkonen, 2002; Hardy *et al*., 2004; Pomeroy *et al*., 2012) which also found greater contributions to melt from turbulent fluxes in the wetlands than the forests, likely as a result of higher wind speeds and a larger air temperature gradient. Reduced windspeeds in forest areas supressed the energy contributions from turbulent heat transfer.

Maximum snow accumulation has been shown to occur in openings two to five times the average height of the surrounding canopy (Golding and Swanson, 1986). Canopy height surrounding the wetlands yields a minimum tree height of 1.6 m and a maximum tree height of 4.5 m. Based on the maximum tree height shown here, snow accumulation would be greatest in openings with a maximum fetch of 25 m, which is still considerably lower than any wetlands where snow surveys were conducted as part of the 9-year period of record. The smallest wetland with annual SWE measurements is a circular feature with an area of ~1000 m^2 and a fetch length of 73 m. Unfortunately, there is insufficient data at this study site to test the hypothesis that small openings retain more snow than forested areas. Helbig *et al*. (2016) found that Scotty Creek is characterized by uniform wind fields, indicating that no accumulation patterns would be expected relative to wind direction.

While the size and shape of surveyed wetlands did not satisfy the areal characteristics required for maximum accumulation, results remained consistent with other studies showing linkages between SWE loss in large openings to wind redistribution and surrounding tree height (Troendle and Leaf, 1980; Golding and Swanson, 1986, Pomeroy *et al*., 2002). Typically, large openings (*i.e.* large WL sites) with a width equal to 20 times the average height of the surrounding trees are more susceptible to wind redistribution and can yield less SWE than a more sheltered forested area (Golding and Swanson, 1986). This phenomenon was apparent at the forest-wetland complex studied, as indicated by the consistently lower SWE (~30%) found in

wetlands when compared to forests (Table 3). This is likely a result of the relatively large size of the wetlands sampled over the 9-year period of record (fetch >163 m; defined as the distance over which the wind can blow unobstructed) and comparatively short, sparse, surrounding canopy (3.1 m). It is important to note, however, that this is not necessarily the case earlier in the winter when the tree canopies are accumulating intercepted snow (Pomeroy *et al*., 2002) as the greater aerodynamic roughness imposed by the tree canopy limits the re-entrainment of deposited snow by the wind.

Findings of this study suggest that relative to the WL and DF sites, SF sites typically receive the highest amount of end of season SWE. The open and relatively thin tree canopy at SF sites is sparse enough to minimize canopy interception, but inhibits turbulent fluxes by preventing wind-driven sublimation and transportation. This is an important distinction between forests in more temperate environments, where a proportionally larger tree canopy can greatly increase interception.

Several studies have noted the existence of a "radiative paradox" to explain the long-wave offset of decreases in shortwave irradiance with increasing canopy density (e.g., Woo and Giebrecht, 2000; Rowlands et al., 2002; Pomeroy et al., 2009). Lawler and Link (2011) suggest the existence of two incoming radiative paradoxes unique to discontinuous forests resultant of variable canopy gaps and changing solar elevation angles. The first paradox suggests that in small gaps, when solar elevation angles are relatively low, the snow surface may remain shaded throughout the day. Increases to longwave radiation remain minimal due to a relatively large sky view fraction resulting in all-wave radiative minima relative to both continuous canopy and open environments. The second paradox indicates a reversal of these conditions at high solar elevation angles. Gaps may receive similar amounts of shortwave radiation as open sites, and similar

longwave radiation amounts as continuous canopy sites due to a relatively small sky view fraction. In this case, all-wave radiation can be higher in the small forest gap relative to both the continuous canopy and open sites, resulting in a radiative 'hotspot' which may be enhanced by warm tree boles that increase longwave emission (Pomeroy et al., 2009).

The phenomenon associated with the first paradox was observed during both years of this study, and is indicated by the ~35% contributions from L* to Q*. Despite this, shortwave reduction caused by the tree canopy was found to be the dominant control on snowmelt energy availability (consistent with Link and Marks, 1999). As a consequence, the snowmelt rate beneath forest canopies was lower than at adjacent treeless terrains (WL sites). Temporal changes in albedo throughout the melt periods were also examined, illustrating the reduction in albedo with time, and increasing forest density likely owing the increase in needle-leaf deposition. With contributions of ~35% from L* to Q*, the difference in albedo between wetland and forested areas served as an important factor affecting changes in land cover specific surface energetics for this study area. Generally, contributions from L* only account for a small fraction of the shortwave that is blocked by the canopy (Metcalfe and Buttle, 1998) and as such, K↓ remains the controlling radiative flux.

While it is not novel to state that K↓ is the dominant flux controlling snowmelt, it is important to examine the implications of this given a changing landscape. The Scotty Creek basin is undergoing a rapid conversion land cover types from forest to wetland in response to permafrost thaw (Quinton *et al*., 2003; Chasmer and Hopkinson, 2016). Under a hypothetical complete conversion of forested plateaus to permafrost-free wetlands, Helbig *et al*. (2016) suggest a near-surface cooling of 3-4 °C in late winter, due to the increase in albedo of a treeless landscape. In this study we show that WL sites lose their snowpack more rapidly than forested

sites. Combining the results of Helbig *et al*. (2016), it may be expected that a hypothetical homogenous, wetland landscape may experience a delayed onset of snowmelt (in response to local cooling), but will lose the snowpack quicker once snowmelt has commenced. A more rapid release of snowmelt water will delay the lag time between snowmelt and peak flows during the spring freshet, producing a flashier hydrograph and providing less storage on the landscape.

2.5.2 Permafrost thaw induced changes to SWE and melt runoff:

The increased proportion of the snow cover that contributes meltwater for landscape runoff to the basin drainage network (*e.g.* channel fens), may also be a factor contributing to the rising annual runoff from streams and rivers in the study region (Connon *et al*., 2014). This possibility is supported by the rising runoff ratios of streams and rivers during the annual snowmelt periods. At Scotty Creek, permafrost thaw results in the transformation of forested peat plateaus (DF and SF) to wetlands (WL). As documented in this study, the mechanisms for snow accumulation and melt are different between these land cover types. As permafrost thaws and the relative proportion of these land cover types change, total SWE accumulation and the timing of the release of meltwater will also change. Furthermore, permafrost thaw has led to increased surface and subsurface connectivity of wetlands that is fundamentally changing the way in which water is routed and stored on the landscape (Connon *et al*., 2014, 2015). Water is routed to the basin outlet through a network of channel fens (Quinton *et al*., 2003; Hayashi *et al*., 2004), which are amalgamating and coalescing with bogs in response to permafrost thaw. This process increases the effective contributing area of the basin and has been shown to increase basin runoff ratios in recent years (Connon *et al*., 2014; Chasmer and Hopkinson, 2016). As a result, the amount of SWE that is made available for runoff upon melt is proposed to increase.

In a change detection analysis, Connon *et al*. (2014) found that for the period 1977 to 2010, total forested area decreased by 7% over a 6 km^2 area at Scotty Creek. End-of-winter SWE has been measured at different land cover types at Scotty Creek for 10 years (2006-2015). Average SWE for each land cover type was calculated over this 10-year period and was used to calculate areally weighted end-of-winter SWE based on the forest (SF and DF) to wetland (WL) ratios for 1977 and 2010. Given a constant input of SWE, but applied to different land cover conditions, total areal SWE decreased by 1.5% (120 mm to 118 mm) over the 33-year period; a negligible change given the inter-annual variability in SWE.

This represents the change in SWE accumulation strictly by change in land cover type and does not include the effects of increased connectivity. Over the same time period (1977-2010), Connon *et al*. (2014) found that the area of the basin capable of transmitting runoff to the basin outlet increased from 31.4% to 41.8%. Using these estimates, the amount of SWE made available as runoff increased by 25% (37 mm to 49 mm) over the 33-year period. The increase in available runoff due to changes in surface and near-surface hydrological connectivity substantially outweighs the decrease caused by transformation of land cover type.

These hydrological changes are evident in increased basin runoff ratios in the lower Liard River valley (Connon *et al*., 2014; Chasmer and Hopkinson, 2016). Collection of stream flow data by the Water Survey of Canada at Scotty Creek began in 1996, and is therefore insufficient in length to analyze change over long time periods. Jean-Marie River, a 1310 km^2 basin located adjacent to Scotty Creek has streamflow data commencing in 1976 and exhibits similar land-cover characteristics to Scotty Creek (Quinton *et al*., 2003). The changing runoff regimes at Jean-Marie River are evident when comparing the 10-year average composite hydrographs for the periods 1976-1985 and 2006-2015 (Figure 7), especially during the spring freshet period.

Average annual runoff more than doubled between the two periods (87 mm to 193 mm), while annual precipitation increased marginally (365 mm to 402 mm). This resulted in a doubling of basin runoff ratios, from 0.24 to 0.48, further illustrating the enhanced efficiency of transporting precipitation inputs to the stream network.

2.6 Conclusions:

Recent work in the wetland-dominated, southern fringe of discontinuous permafrost has demonstrated that the relative proportions and spatial arrangement of land cover types within this zone is changing due to climate warming. This warming-induced land-cover change is changing the water balance at basin and regional scales.

Our results demonstrate that permafrost thaw in the study region is changing how snowmelt is partitioned between storage and runoff with potentially important implications for water resources. Here, we have characterized the snow cover and melt regimes over three characteristic terrain types; wetland, sparse forest, and dense forest. We have evaluated the effect of changes to tree-covered area and canopy density on the volume and timing of snowmelt at the end of winter. This information has demonstrated that permafrost thaw driven conversion of forests to treeless wetlands has marginally decreased areal SWE while increasing the amount of SWE made available as runoff. The increase in available runoff due to changes in surface and near-surface hydrological connectivity substantially outweighs the decrease caused by transformation of land cover type.

The partitioning of these land cover types based on energetics and accumulation and melt patterns poses important implications to water resources should land cover change continue to occur. Since K↓ was found to be a controlling radiative flux it can be reasoned that open areas will lose snow more quickly than forested areas. Should permafrost thaw driven land cover

conversion from forest to wetland continue, we predict to see a more rapid snowmelt and in turn, more exposed ground cover for a longer duration which could lead to increased thaw rates. Hydrologically, this could have implications for the volume and timing of runoff (flashier hydrographs with higher spring peaks) and influence the rate and spatial pattern of permafrost thaw. As there is a dearth of knowledge on the quantification of the variation of melt rates and snow cover depletion in the fringe zone by field measurements during melt, more studies like this are required to be able to better simulate snowmelt, ground thaw, and runoff for this region.

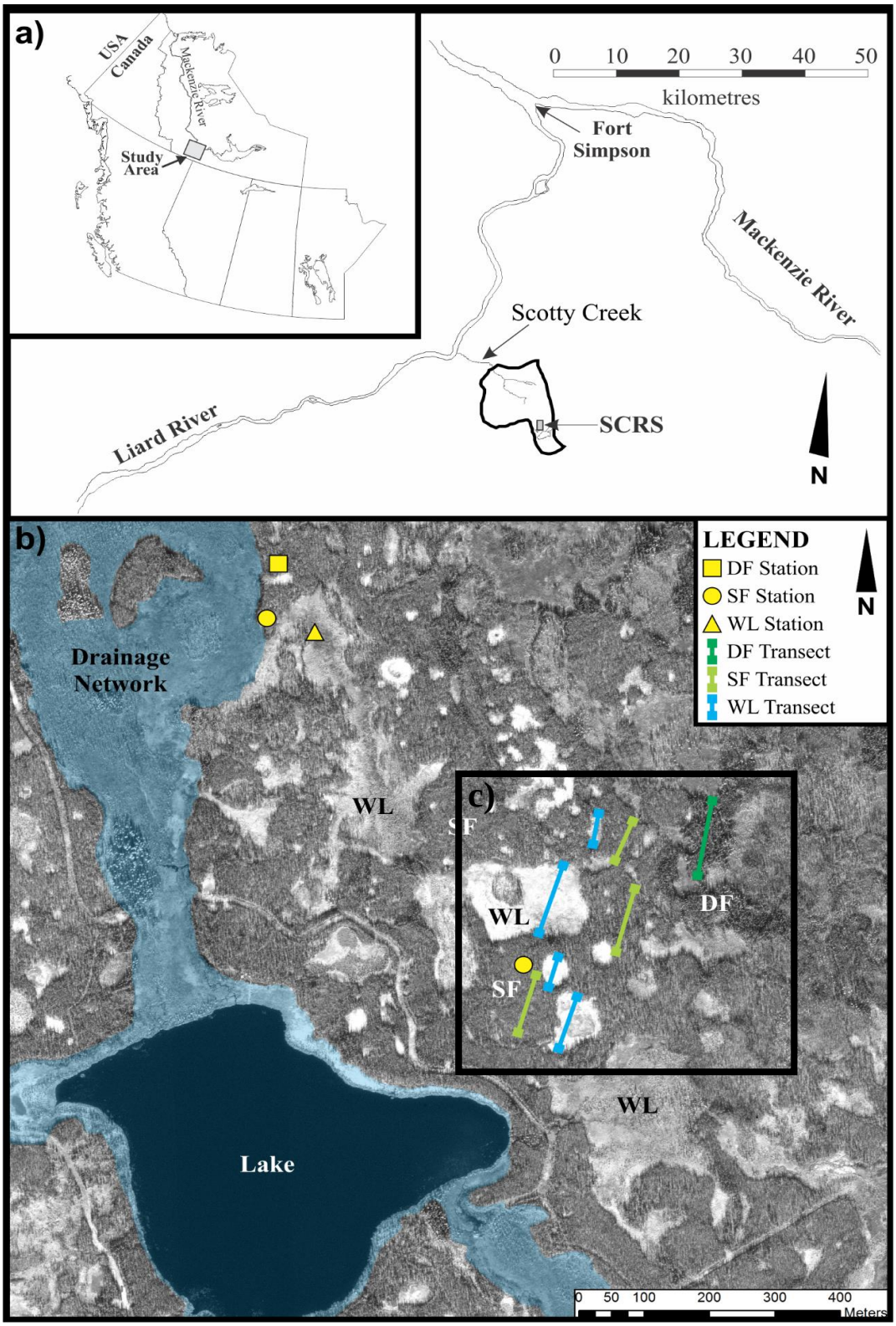

Figure 1. (a) Location of study site. **(b)** Classified 22 km ^{2} image of the Scotty Creek basin illustrating location of meteorological stations used in study. **c)** 0.14 km^2 area-of-interest (AOI) with 40% forest and 60% wetland coverage.

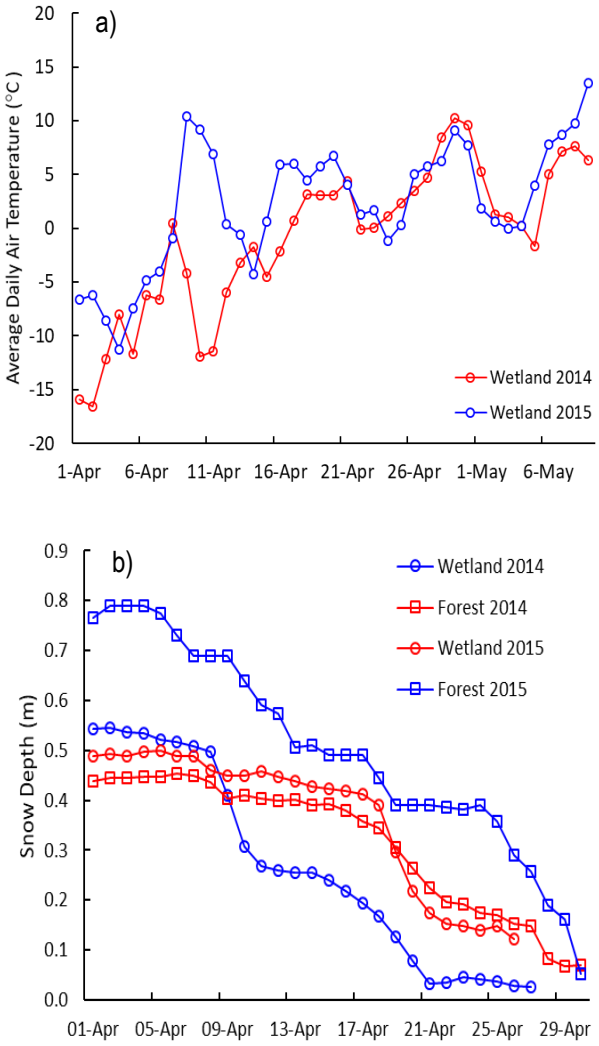

Figure 2. Average daily air temperature (Ta), experienced at Scotty Creek; (**b)** Line plot illustrating change in snow depth (m) throughout the 2014 and 2015 melt seasons for the forest and wetland land cover types.

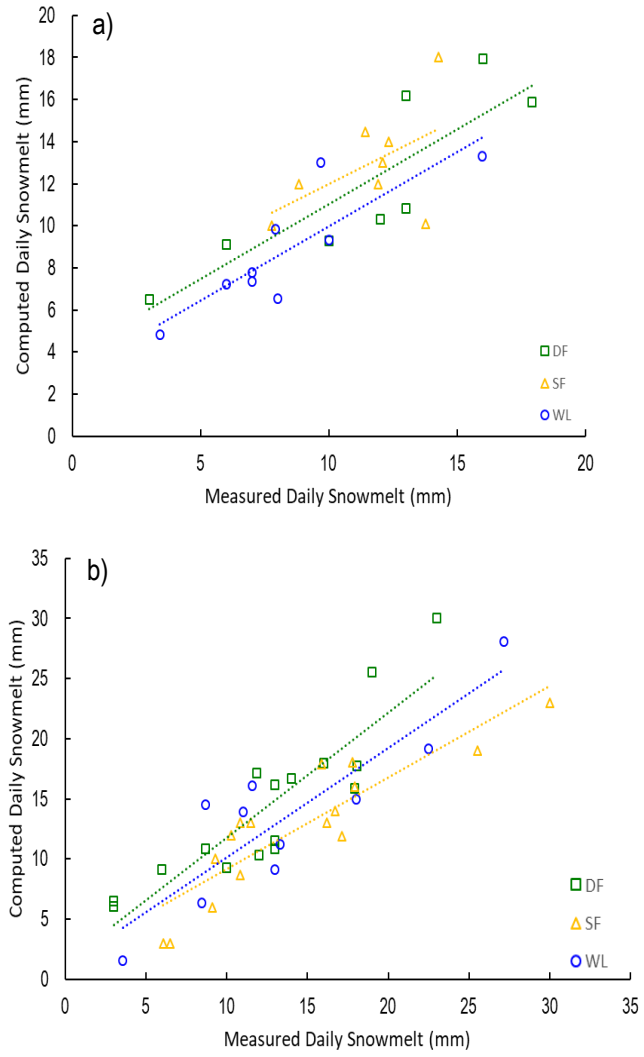

Figure 3. Scatterplots illustrating measured and computed daily total melt rates in mm for WL, SF, and DF sites in **(a)** 2014; R^2 = 0.73, 0.74, 0.51 and **(b)** 2015; R^2 = 0.85, 0.76, 0.68.

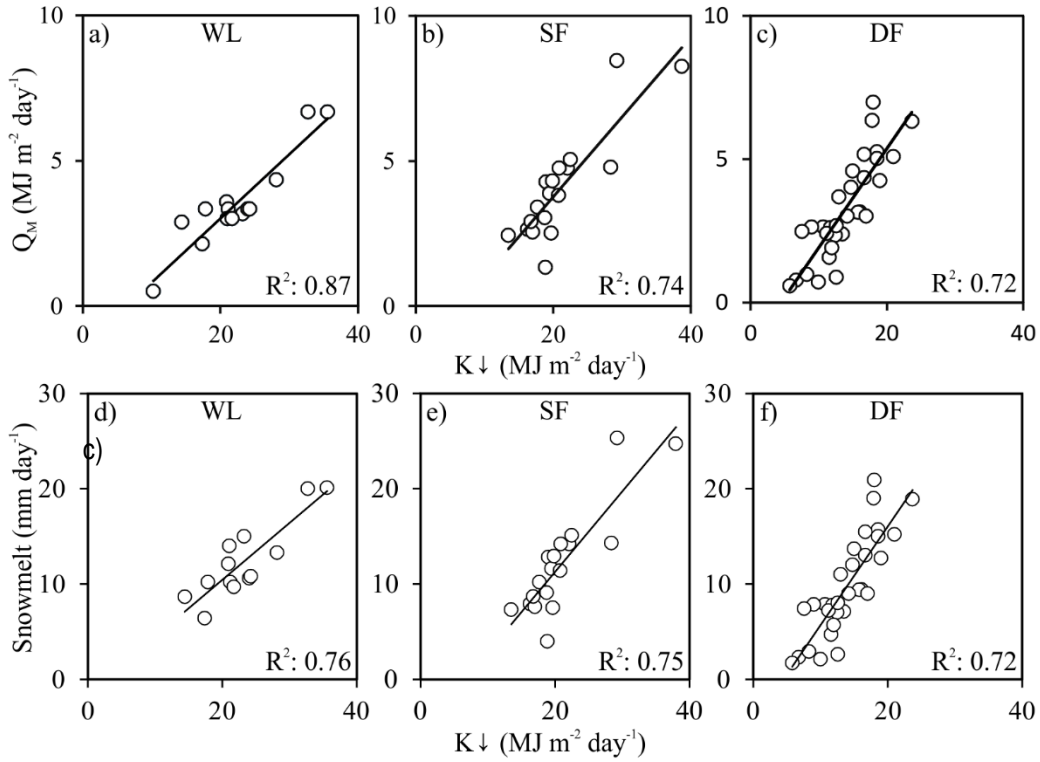

Figure 4. (a) Scatterplot illustrating agreement between total daily snowmelt energy and modelled total daily K↓, both in megajoules for the various transect locations (WL>SF> >DF; R^2 = 0.64 to 0.87). Scatter plots illustrating relationship between computed daily snowmelt and total daily measured K↓ for 2014 and 2015. K↓ was found to be the dominant flux contributing to snowmelt for all land cover types studied.

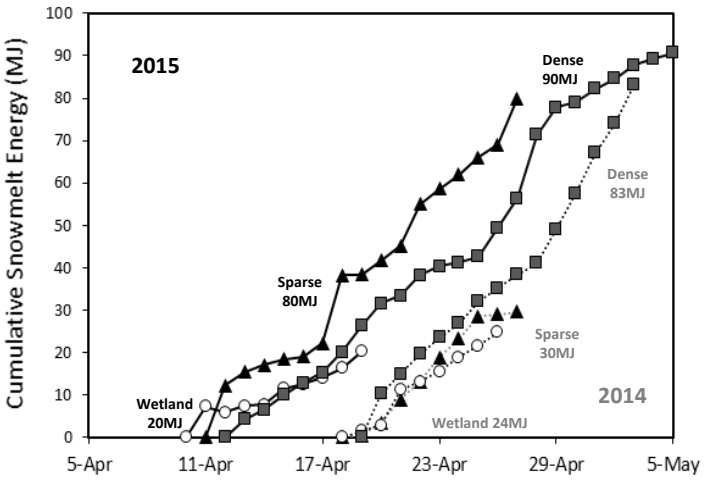

Figure 5. Line plot illustrating cumulative snowmelt energy in megajoules for the 2014 and 2015 periods of study for wetland, sparse forest, and dense forest land cover types.

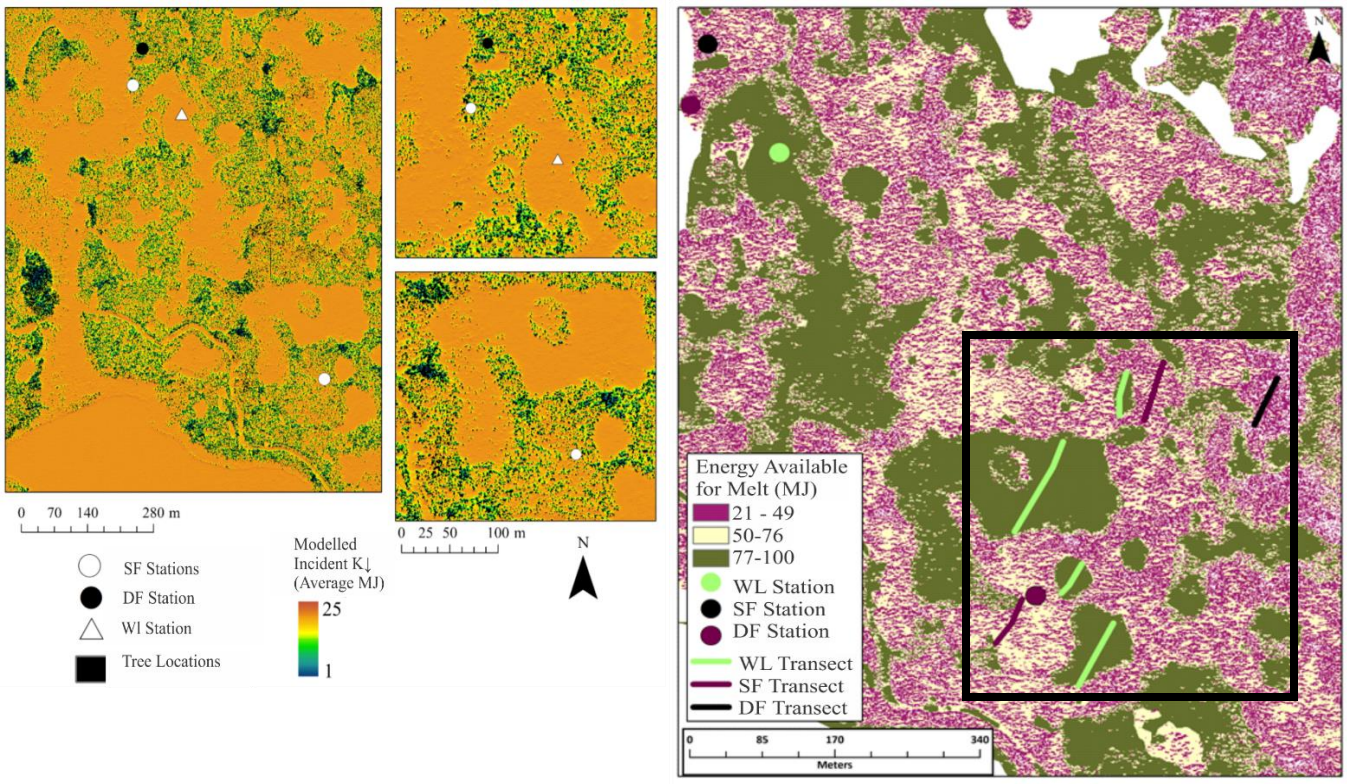

Figure 6. (a) Location of trees combined and distribution of incoming solar radiation to the ground for the study periods in megajoules. **(b)** Image inset presents 0.14 km^2 AOI illustrating routinely surveyed snow transects, location of meteorological stations used in study, as well as the distribution of snowmelt energy in megajoules based on cumulative daily modelled incoming shortwave radiation receipt to the ground.

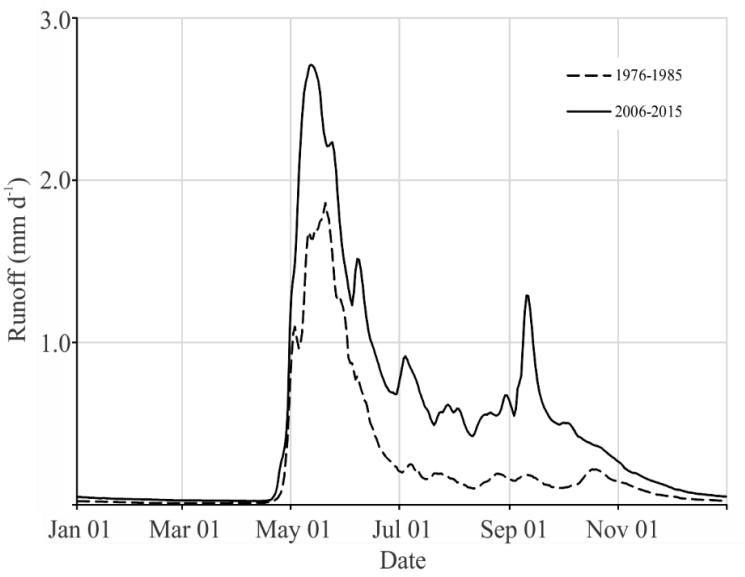

Figure 7. Composite hydrograph of Jean-Marie River for the time periods 1976-1985 and 2006-2015.

Table 1. Average depth, density, and SWE for each landcover type. Values were computed based on data collected through routine snow surveying for the end of winter snowmelt in 2014 and 2015; Geonor data was obtained and adjusted from the Scotty Creek Research Station.

	Gauge SWE		Snow Survey SWE		Snow Survey Depth						Snow Survey Density					
	Scotty Creek	Fort Simpson	WL	Forest	WL			Forest			WL			Forest		
Year	(mm)	(mm)	(mm)	(mm)	$\bar{x}$ (cm)	σ (cm)	n	$\bar{x}$ (cm)	σ (cm)	n	$\bar{x}$ (g cm^{-3})	σ (g cm^{-3})	n	$\bar{x}$ (g cm^{-3})	σ (g cm^{-3})	n
2014	143.7	95.6	95.8	99.1	60.1	5.7	206	58.3	6.8	215	0.159	0.025	48	0.170	0.029	38
2015	216.6	167.0	170.8	179.9	69.5	8.6	127	69.5	10.8	79	0.246	0.036	31	0.232	0.038	19

Table 2. Snow cover duration period.

Year	Land Cover	Start	End	Days
2014	DF	18 Apr	01 May	13
	SF	18 Apr	27 Apr	9
	WL	18 Apr	26 Apr	8
2015	DF	12 Apr	05 May	23
	SF	11 Apr	27 Apr	16
	WL	10 Apr	20 Apr	10

Table 3. 2014 and 2015 total snowfall values for Scotty Creek and Fort Simpson.

	2014		2015	
	Scotty Creek	Fort Simpson	Scotty Creek	Fort Simpson
Month	Corrected (mm)	Raw (mm)	Corrected (mm)	Raw (mm)
October	11.5	6.2	46.2	40.8
November	27.7	20.4	29.0	20.6
December	26.5	19.6	14.7	21.6
January	46.4	30.6	30.0	15.4
February	9.7	6.2	50.4	39.0
March	11.4	4.0	22.5	19.0
April	8.6	5.0	22.7	10.0
May	2.0	3.6	1.3	0.6
Annual	143.7	95.6	216.6	167.0

Table 4. Percent contribution from each computed energy balance component to the total energy available for melt; absolute values taken for fluxes expressed as an energy loss from the snowpack.

Year	Land Cover	Q_e	Q_h	Q*
2014	DF	8	12	80
	SF	10	10	80
	WL	15	17	68
2015	DF	8	16	75
	SF	8	5	87
	WL	12	18	70

Chapter 3:

3.1 Summary and Conclusions:

Recent global climate trends suggest evidence of a northward migration of atmospheric moisture (Peterson, et al., 2002). This makes the investigation of snow accumulation and melt in regions dominated by these processes to be of greater concern due to the implications on the frequency and form of precipitation events (Peterson, et al., 2002).

At high latitudes, snow has a significant influence on hydrological and atmospheric processes. Large portions of these regions are covered by evergreen coniferous forests which affect energy and mass exchanges between the atmosphere, canopy, and ground surface (Eaton *et al*., 2001). Beneath a forest canopy, energy budget dynamics are strongly influenced by the large spatial variability of radiative and turbulent transfers (Pomeroy *et al*., 2008). The spatial variation of shortwave irradiance to snow is important to quantify as it can affect the depletion of snow covered area and areal melt rates (Pomeroy *et al*., 2008). However, the magnitude of this variation has been sparsely quantified by field measurements during melt. The spatial variability of melt energy derived from radiation on cloudy days has been shown to be vastly different from that experienced on sunny days highlighting the variability in downwelling radiant energy, (Rowlands *et al*., 2002).

The degree of influence to which radiative and turbulent transfers are affected is dependent on the structure of the forest canopy and density (Hardy *et al*., 2004). For instance, trees pose substantial implications to the spatial distribution of melt energy. Trees attenuate a large part of the incoming solar radiation, shelter the snow surface from wind, and thereby reduce the amount of energy available for melt by dampening turbulent fluxes; making snowmelt dependent mainly on radiative fluxes (Boon *et al*., 2009; Davis et al., 1997). Additionally, trees

alter snow surface albedo in that leaf litter deposited onto the snow surface will increase with increasing canopy cover and lead to increased melt rates (Sicart et al., 2003).

While canopy density and structure have been identified as primary factors affecting the spatial distribution of radiative fluxes, studies have also shown forest canopy disturbance to be a controlling factor in generating peak streamflows (Burles and Boon, 2011). This is due to the decrease in sublimation loss from interception and blowing snow from the forest canopy, (Burles and Boon, 2011; Pomeroy *et al*., 2012). Furthermore, Eaton (2001) has shown a clear correspondence between energy balance characteristics and terrain types after examining the surface energy balance of five sites across western and subarctic Canada, and the major variations between these terrain types.

These studies highlight the variability in surface energetics across a landscape, and the subsequent importance of developing an accurate characterization of the radiation regime beneath a forest canopy. This is necessary for the parameterization of physically-based canopy models, as well as for the assessment of variability in short and longwave radiative components, as well as for input to energy-balance models concerned with ground conditions beneath a canopy (Pomeroy *et al*., 2009). As this region remains snow covered for most of the year, and the end of winter snowmelt event produces the most prominent feature of stream hydrographs in cold regions, changes to basin snow covers resulting from permafrost thaw-induced land cover change have the potential to disrupt the hydrological cycle of basins throughout the fringe zone. Therefore, in order to understand the long-term implications of land-cover changes occurring throughout this region on late-winter snow distribution, melt and runoff, it is necessary to understand how the major land cover types of this region differ with respect to their snow covers and their rates and patterns of snowmelt.

Here, I have characterized the snowcover and snowmelt regimes over a spectrum from treeless terrains to dense canopies. Using this information, I have evaluated the effect of changes to tree-covered area and canopy density on the volume and timing of snowmelt at the end of winter. Analysis of historical imagery suggests that wetland coverage within a 0.14-km^2 area-of-interest increased by approximately 7 % between 1977 and 2010. Over the 34-year period, total areal SWE decreased by 1.5 %, but the amount of SWE made available as runoff increased by 25%. The increased proportion of the snow cover that contributes melt water to streams may be a factor contributing to the rising steam flows observed across the study region in the mid-1990s and early 2000s, given that there has been no concomitant increase in winter-time precipitation.

This could pose substantial implications for water resources and management within the region should climate change continue. As there is a deficit of knowledge on the quantification of the variation of melt rates and snow cover depletion in the fringe zone by field measurements during melt, more studies like this are required to be able to better simulate snowmelt, ground thaw and runoff for this region.

3.2 References

Andreas, E. L. (2002). Parameterizing scalar transfer over snow and ice: a review. *Journal of Hydrometeorology*, *3*(4), 417-432.

Aylesworth, J. M., & Kettles, I. M. (2000). Distribution of fen and bog in the Mackenzie Valley, 60N. *Natural Resources Canada, Geological Survey of Canada Bulletin, 547*.

Baltzer, J. L., Veness, T., Chasmer, L. E., Sniderhan, A. E., & Quinton, W. L. (2014). Forests on thawing permafrost: fragmentation, edge effects, and net forest loss. *Global Change Biology*, *20*(3), 824-834.

Beilman, D.W., and Robinson, S.D. (2003). Peatland permafrost thaw and landform type along a climatic gradient. *In* Proc. 8th Int. Conf. on Permafrost, Zurich, Switzerland, 21–25 July 2003. *Edited by* N. Ross. pp. 61–65.

Boon S. (2009). Snow ablation energy balance in a dead forest stand. *Hydrological Processes, 23*(18), 2600–2610.

Burles, K., & Boon, S. (2011). Snowmelt energy balance in a burned forest plot, Crowsnest Pass, Alberta, Canada. *Hydrological processes*, *25*(19), 3012-3029.

Chasmer, L., Hopkinson, C., Treitz, P., McCaughey, H., Barr, A., & Black, A. (2008). A lidar-based hierarchical approach for assessing MODIS fPAR. *Remote Sensing of Environment*, *112*(12), 4344-4357.

Chasmer, L, Hopkinson C, & Quinton W, 2010. Quantifying errors in discontinuous permafrost plateau change from optical data, Northwest Territories, Canada: 1947-2008. Canadian Journal of Remote Sensing, *36*(2), 211–223.

Cline, D. W. (1997). Snow surface energy exchanges and snowmelt at a continental, midlatitude Alpine site. *Water Resources Research, 33*(4), 689-701.

Connon, R. F., Quinton, W. L., Craig, J. R., & Hayashi, M. (2014). Changing hydrologic connectivity due to permafrost thaw in the lower Liard River valley, NWT, Canada. *Hydrological Processes, 28*(14), 4163-4178.

Connon, R. F., Quinton, W. L., Craig, J. R., Hanisch, J., & Sonnentag, O. (2015). The hydrology of interconnected bog complexes in discontinuous permafrost terrains. *Hydrological Processes*, *29*(18), 3831-3847.

Davis, R. E., J.P. Hardy, W. Ni, C. Woodcock, J. C. McKenzie, R. Jordan, and X. Li. (1997) Variation of snow cover ablation in the boreal forest: A sensitivity study on the effects of conifer canopy, *J. Geophys. Res*., *102*(29), 389-395.

Devine, K. A., & Mekis, É. (2008). Field accuracy of Canadian rain measurements. *Atmosphere-Ocean*, *46*(2), 213-227.

Dingman, S. L. (2002). Physical hydrology, Chapter 5: snow and snowmelt, 159–209.

Ellis, C. and Pomeroy, J. (2007). Estimating sub-canopy shortwave irradiance to melting snow on forested slopes. *Hydrological Processes, 21*(19), 2581-2593.

Essery, R., Li, L., & Pomeroy, J. (1999). A distributed model of blowing snow over complex terrain. *Hydrological processes*, *13*(1415), 2423-2438.

Faria, D. A., Pomeroy, J. W., & Essery, R. L. H. (2000). Effect of covariance between ablation and snow water equivalent on depletion of snow-covered area in a forest. *Hydrological Processes*, *14*(15), 2683-2695.

Garon-Labrecque M-E, Léveillé-Bourret É, Higgins K, Sonenetag O. (2015). Additions to the boreal flora of the Northwest Territories with a preliminary vascular flora of Scotty Creek. *Canadian Field-Naturalist*, *129*(4), 349-367.

Garnier, BJ and Ohmura A. (1968). A method of calculating the direct shortwave radiation income of slopes. *Journal of Applied Meteorology*, *7*(5), 796-800.

Gelfan, A. N., Pomeroy, J. W., & Kuchment, L. S. (2004). Modeling forest cover influences on snow accumulation, sublimation, and melt. *Journal of Hydrometeorology*, *5*(5), 785-803.

Gibson, J. J., Edwards, T. W. D., & Prowse, T. D. (1993). Runoff generation in a high boreal wetland in northern Canada. *Hydrology Research*, *24*(2-3), 213-224.

Golding, D. L., & Swanson, R. H. (1986). Snow distribution patterns in clearings and adjacent forest. *Water Resources Research*, *22*(13), 1931-1940.

Goodrich, L. E. (1982). The Influence of Snow Cover on the Ground Thermal Regime', Canadian Geotechnical Journal, *19*(4), 412–432.

Granger, R. J., Essery, R., & Pomeroy, J. W. (2006). Boundary-layer growth over snow and soil patches: field observations. *Hydrological Processes*, *20*(4), 943-951.

Harding, R. J., & Pomeroy, J. W. (1996). The energy balance of the winter boreal landscape. *Journal of Climate*, *9*(11), 2778-2787.

Hardy, J. P., Melloh, R., Koenig, G., Marks, D., Winstral, A., Pomeroy, J. W., & Link, T. (2004). Solar radiation transmission through conifer canopies. *Agricultural and forest meteorology*, *126*(3), 257-270.

Heron, R., & Woo, M. K. (1978). Snowmelt computations for a high Arctic site. In *Proceedings of the 35th Eastern Snow Conference, Hanover, New Hampshire* (pp. 162-172).

Hinzman, L. D., Bettez, N. D., Bolton, W. R., Chapin, F. S., Dyurgerov, M. B., Fastie, C. L., & Jensen, A. M. (2005). Evidence and implications of recent climate change in northern Alaska and other arctic regions. *Climatic Change*, *72*(3), 251-298.

Hopkinson, C. and Chasmer, L. (2009). Testing a lidar intensity based model of canopy fractional cover across multiple forest ecozones. *Remote Sensing of Environment*, *113*(1), 275-288.

Intergovernmental Panel on Climate Change (IPCC), (2014), Climate Change 2014: Synthesis Report, *Contribution of Working Groups I, II and III to the Fifth Assessment Report of the Intergovernmental Panel on Climate Change* [Core Writing Team, R.K. Pachauri and L.A. Meyer (eds.)], IPCC, Geneva, Switzerland, 151 pp.

Jorgenson MT, Racine CH, Walters JC, Osterkamp TE. (2001). Permafrost degradation and ecological changes associated with a warming climate in central Alaska. *Climatic Change*, *48*(4), 551-579.

Jorgenson MT and Osterkamp TE. (2005). Response of boreal ecosystems to varying modes of permafrost degradation. *Canadian Journal of Forest Research*, *35*(9), 2100–2111.

Jorgenson, M. T., Romanovsky, V., Harden, J., Shur, Y., O'Donnell, J., Schuur, E. A., & Marchenko, S. (2010). Resilience and vulnerability of permafrost to climate change This article is one of a selection of papers from The Dynamics of Change in Alaska's Boreal Forests:

Resilience and Vulnerability in Response to Climate Warming. *Canadian Journal of Forest Research*, *40*(7), 1219-1236.

Marchenko, S. (2010). Resilience and vulnerability of permafrost to climate change. *Canadian Journal of Forest Research*, *40*(7), 1219-1236.

Knox, S. H., Carey, S. K., & Humphreys, E. R. (2012). Snow surface energy exchanges and snowmelt in a shrub-covered bog in eastern Ontario, Canada. *Hydrological Processes*, *26*(12), 1876-1890.

Koivusalo, H., & Kokkonen, T. (2002). Snow processes in a forest clearing and in a coniferous forest. *Journal of Hydrology*, *262*(1), 145-164.

Kort, J., Bank, G., Pomeroy, J., & Fang, X. (2012). Effects of shelterbelts on snow distribution and sublimation. *Agroforestry systems*, *86*(3), 335-344.

Kruskal, W. H., & Wallis, W. A. (1952). Use of ranks in one-criterion variance analysis. *Journal of the American Statistical Association*, *47*(260), 583-621.

Kwong, Y. J., & Gan, T. Y. (1994). Northward migration of permafrost along the Mackenzie Highway and climatic warming. *Climatic Change*, *26*(4), 399-419.

Lantz, T. C., & Kokelj, S. V. (2008). Increasing rates of retrogressive thaw slump activity in the Mackenzie Delta region, NWT, Canada. *Geophysical Research Letters*, *35*(6).

Liston, G. E., & Sturm, M. (2002). Winter precipitation patterns in arctic Alaska determined from a blowing-snow model and snow-depth observations. *Journal of hydrometeorology*, *3*(6), 646-659.

Magnussen, S., and Boudewyn, P. 1998. Derivations of stand heights from airborne laser scanner data with canopy-based quantile estimators. *Canadian Journal of Forest Research, 28*(7), 1016-1031.

Male, D. H., & Granger, R. J. (1981). Snow surface energy exchange. *Water Resources Research*, *17*(3), 609-627.

McClymont AF, Hayashi M, Bentley L, Christensen B. (2013). Geophysical imaging and thermal modeling of subsurface morphology and thaw evolution of discontinuous permafrost. *Journal of Geophysical Research: Earth Surface*, *118*(3), 1–12.

Mekis, É., & Vincent, L. A. (2011). An overview of the second generation adjusted daily precipitation dataset for trend analysis in Canada.*Atmosphere-Ocean*, *49*(2), 163-177.

Metcalfe, R. A., & Buttle, J. M. (1998). A statistical model of spatially distributed snowmelt rates in a boreal forest basin. *Hydrological Processes*, *12*(1011), 1701-1722.

Meteorological Service of Canada (MSC), 2016. National climate data archive of Canada. Environment Canada: Dorval, Quebec, Canada.

Moore, R. D. (1983). On the use of bulk aerodynamic formulae over melting snow. *Hydrology Research*, *14*(4), 193-206.

Morsdorf, F., Kotz, B., Meier, E., Itten, K.I., Allgower. B. (2006). Estimation 1 of LAI and fractional cover from small footprint airborne laser scanning data based on gap fraction. *Remote Sensing of Environment*, *104*(1), 50-61.

O'Sullivan, D. and D.J. Unwin, 2003. Geographic Information Analysis. Wiley. Hoboken, NJ.

Oke, T. R. (2002). *Boundary layer climates*. Routledge.

Pachauri, R. K., & Reisinger, A. (Eds.). (2007). *Climate change 2007 synthesis report: Summary for policymakers*. IPCC Secretariat.

Peterson, B. J., Holmes, R. M., McClelland, J. W., Vörösmarty, C. J., Lammers, R. B., Shiklomanov, A. I., ... & Rahmstorf, S. (2002). Increasing river discharge to the Arctic Ocean. S*cience*, *298*(5601), 2171-2173.

Pomeroy, J. W., & Gray, D. M. (1995). Snowcover accumulation, relocation and management. *Bulletin of the International Society of Soil Science no*, *88*(2).

Pomeroy, J. W., Bewley, D. S., Essery, R. L. H., Hedstrom, N. R., Link, T., Granger, R. J., ... & Janowicz, J. R. (2006). Shrub tundra snowmelt. *Hydrological Processes*, *20*(4), 923-941.

Pomeroy, J., Ellis, C., Rowlands, A., Essery, R., Hardy, J., Link, T., ... & Sicart, J. E. (2008). Spatial variability of shortwave irradiance for snowmelt in forests. *Journal of Hydrometeorology*, *9*(6), 1482-1490.

Pomeroy, J. W., Marks, D., Link, T., Ellis, C., Hardy, J., Rowlands, A., & Granger, R. (2009). The impact of coniferous forest temperature on incoming longwave radiation to melting snow. *Hydrological Processes*, *23*(17), 2513-2525.

Pomeroy, J., Fang, X., & Ellis, C. (2012). Sensitivity of snowmelt hydrology in Marmot Creek, Alberta, to forest cover disturbance. *Hydrological Processes*, *26*(12), 1891-1904.

Price, A. G., & Dunne, T. (1976). Energy balance computations of snowmelt in a subarctic area. *Water Resour. Res*, *12*(4), 686-694.

Putkonen, J., Grenfell, T. C., Rennert, K., Bitz, C., Jacobson, P., & Russell, D. (2009). Rain on snow: little understood killer in the north. *Eos, Transactions American Geophysical Union*, *90*(26), 221-222.

Quinton, W. L., Hayashi, M., & Pietroniro, A. (2003). Connectivity and storage functions of channel fens and flat bogs in northern basins. *Hydrological Processes*, *17*(18), 3665-3684.

Quinton, W. L., Hayashi, M., & Chasmer, L. E. (2009). Peatland hydrology of discontinuous permafrost in the Northwest Territories: overview and synthesis. *Canadian Water Resources Journal*, *34*(4), 311-328.

Quinton, W. L., Hayashi, M., & Chasmer, L. E. (2011). Permafrost-thaw-induced land-cover change in the Canadian subarctic: implications for water resources. *Hydrological Processes*, *25*(1), 152-158.

Quinton, W. L., & Baltzer, J. L. (2013). The active-layer hydrology of a peat plateau with Hardy, J. P., Melloh, R., Koenig, G., Marks, D., Winstral, A., Pomeroy, J. W., & Link, T. (2004). Solar radiation transmission through conifer canopies. *Agricultural and forest meteorology*, *126*(3), 257-270.

Shapiro, S. S., Wilk, M. B., & Chen, H. J. (1968). A comparative study of various tests for normality. Journal of American Statistical Association, *63*(324), 1343-1372.

Smith, C. G., 2008: Correcting the wind bias in snowfall measurements made with a Geonor T-200B precipitation gauge and alter wind shield. CMOS Bull., 36, 162–167.

Sicart, J. E., Essery, R. L., Pomeroy, J. W., Hardy, J., Link, T., & Marks, D. (2004). A sensitivity study of daytime net radiation during snowmelt to forest canopy and atmospheric conditions. *Journal of Hydrometeorology*, *5*(5), 774-784.

St Jacques, J. M., & Sauchyn, D. J. (2009). Increasing winter baseflow and mean annual streamflow from possible permafrost thawing in the Northwest Territories, Canada. *Geophysical Research Letters*, *36*(1).

Storck, P. (2000). Trees, snow, and flooding: An investigation of forest canopy effects on snow accumulation and melt at the plot and watershed scales in the pacific northwest (Order No. 9964293). Available from ProQuest Dissertations & Theses A&I; ProQuest Dissertations & Theses Global. (304638040).

Trochim, E. D., Mumm, J. P., Farnham, N. E., Kane, D. L., & Prakash, A. (2010). Variations in Vegetation & Hydrology: Linkages to Evapotranspiration in the Alaskan Arctic. In *AGU Fall Meeting Abstracts*, 1, 1087.

Troendle, C. A., & King, R. M. (1985). The effect of timber harvest on the Fool Creek watershed, 30 years later. *Water Resources Research*, *21*(12), 1915-1922.

Vines, R. G. (1968). Heat transfer through bark, and the resistance of trees to fire. *Australian Journal of Botany*, *16*(3), 499-514.

Vincent, L. A., Zhang, X., Brown, R. D., Feng, Y., Mekis, E., Milewska, E. J. & Wang, X. L. (2015). Observed trends in Canada's climate and influence of low-frequency variability modes. *Journal of Climate*, *28*(11), 4545-4560.

Woo, M. K., & Giesbrecht, M. A. (2000). Simulation of snowmelt in subarctic spruce woodland: 1. Tree model. *Water Resources Research*, *36*(8), 2275-2285

Woo, M. K. (2012). Snow cover. In *Permafrost Hydrology* (pp. 119-161). Springer Berlin Heidelberg.

Wright, N., Hayashi, M., & Quinton, W. L. (2009). Spatial and temporal variations in active layer thawing and their implication on runoff generation in peat-covered permafrost terrain. *Water Resources Research*, *45*(5).

Zoltai, S. C. (1993). Cyclic development of permafrost in the peatlands of northwestern Alberta, Canada. *Arctic and Alpine Research*, *25*(3), 240-246.